Supplementary Materials for

Evidence for Microbial Carbon and Sulfur Cycling in Deeply Buried Ridge Flank Basalt

Mark A. Lever,* Olivier Rouxel, Jeffrey C. Alt, Nobumichi Shimizu, Shuhei Ono,
Rosalind M. Coggon, Wayne C. Shanks, III, Laura Lapham, Marcus Elvert,
Xavier Prieto-Mollar, Kai-Uwe Hinrichs, Fumio Inagaki, Andreas Teske*

*To whom correspondence should be addressed.
E-mail: mark.lever@biology.au.dk (M.A.L.); teske@email.unc.edu (A.T.)

This PDF file includes:

Materials and Methods

    Sample collection. Basalt cores from borehole U1301B were sampled using a Rotary Core Barrel (RCB) (*9*). Freshly recovered, intact whole-round basalt cores were decontaminated, cracked aseptically, and subsampled to measure drilling fluid contamination (*31*). For DNA extractions, only rock samples were used in which drilling fluid contamination was minimal (<2 contaminant cells g^{-1} basalt) (*31*). This limited analyses to rocks with small, smectite-dominated cross-cutting veins, which – unlike carbonate-dominated major veins - remained intact during drilling, and could be cracked open and aseptically sampled shipboard after core recovery. All processed samples were stored at -80°C prior to extraction of DNA in the home laboratory.

    DNA Extraction. Using sterile spatulas, 2-4 cm^2 (0.3-0.5 g) of inner vein surfaces were scraped off and DNA extracted following the same protocol as previously for RNA (*32*) except that the sodium phosphate (NaH_2PO_4) concentration of the extraction buffer was raised to 120 µM, the pH of the extraction buffer and phenol increased to 8.0, and bead-beating reduced to 15 s at a speed of 4.0. Negative controls containing no basalt samples were run in parallel to check for contamination of extraction reagents. Samples and controls were purified with the PowerClean DNA Clean-Up Kit (MOBIO laboratories, Carlsbad, CA).

    Primer Selection and PCR Amplification. *mcrA* was PCR-amplified using the mcrIRD and ANME-1-mcrI primer pairs. These primer pairs target all known and several novel *mcrA* gene clusters when used complementarily, as shown in extensive tests with marine sediment samples (*33*). *dsrB* was PCR-amplified by nested PCR with published external primers (DSR1F/4R) (*14*), and a newly designed primer mixture used internally (dsrB F1a-h/4RSI1a-f), after tests with published primers had produced negative results (Tables S12 and S13). The PCR protocol consisted of (1) 1×2 min denaturation (98°C), (2) 40× (a) 30s denaturation (95°C), (b) 30s annealing (mcrIRD: 55°C; ANME-1-mcrI: 63°C; DSR1F/4R: 54°C, dsrB F1a-h/4RSI1a-f: 56°C), (c) 1 min extension (72°C), and (3) 1×5 min extension (72°C). In each PCR assay, negative controls for contamination of extraction and PCR reagents were run and found to be negative.

    Cloning, sequencing, and phylogenetic analyses. PCR fragments were purified in a 2% low-melting point agarose gel and agarose removed with a S.N.A.P. MiniPrep Kit. Purified DNA was cloned and inserted into electrocompetent *E. coli* using the TOPO TA Kit (both kits by Invitrogen, Carlsbad, USA). All trees were constructed with nucleotides in ARB Neighbour Joining using Jukes-Cantor correction (*34*).

    Nucleotide sequence accession numbers. The GenBank nucleotide accession numbers are GU182109-GU182110, and JX465656-JX465658.

    Solid-phase S Analyses. Contents and $\delta^{34}S$-compositions of bulk S pools (AVS, CRS, SO_4-S) were analyzed on rock powders using published protocols (*5, 23*).

    The $\delta^{34}S$ of pyrite grains was measured on polished rock thin-sections by SIMS using the mono-collection Cameca IMS 1280 (*35*), and by LA-MC-ICPMS (Laser Ablation Multiple Collector Inductively Coupled Plasma Mass Spectrometry) using the NewWave UP213 laser coupled to the Neptune (Thermo) MC-ICP-MS (*36*). For both techniques, the minimum grain diameter for $\delta^{34}S$-determination was 10µm. In certain samples (e.g. 14R-1, 17R-1, 19R-1), pyrite grains were measured with SIMS and LA-
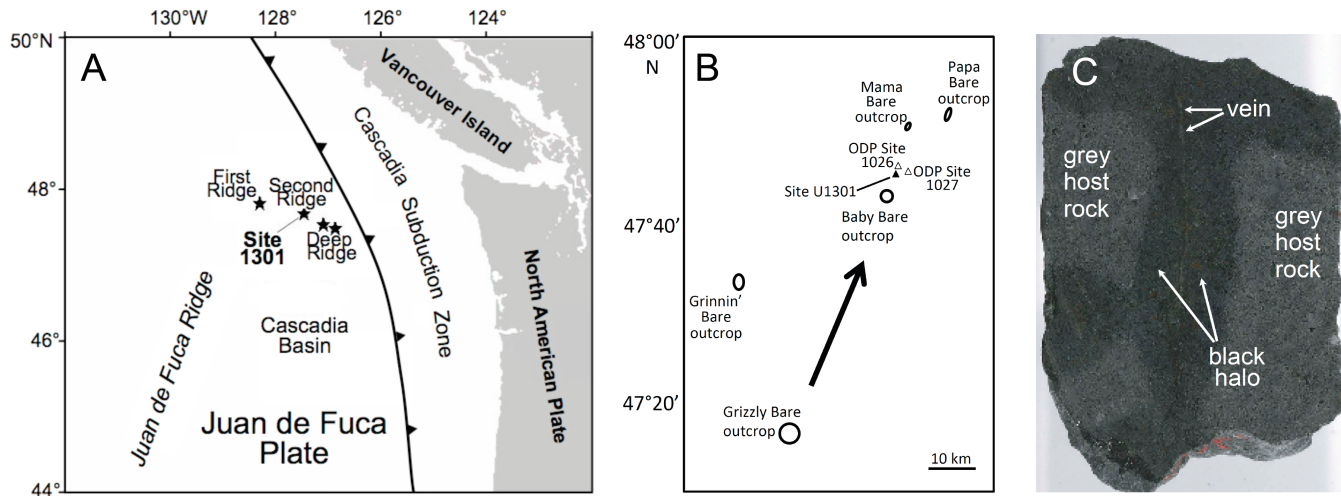
MC-ICPMS and showed agreement within analytical uncertainties. Details of both techniques are outlined in the following paragraphs.

For the SIMS technique, a beam of $^{133}Cs^+$ ions was used for sputter-ionizing S as negatively charged secondary ions from pyrite grains. A mass resolving power (MRP) of ~5000 was used with a primary Cs^+ beam current switched to a spot of ~2 mm diameter with a current of ~6 pA. Peak calibration and pre-sputtering was made for each spot analysis and the intensity data was then processed by an off-line time-interpolation correction protocol to minimize the effect of variations of the primary beam intensity on measured isotope ratios. Pyrite standards used were: Ruttan (+1.2 ‰ VCDT), MVE04-14-4 (-13.15‰), and Balmat (+15.1‰). For each session, at least two of each were measured repeatedly to ascertain that the instrumental mass fractionation factor (a) was statistically identical for all standards. a varied from session to session and day to day, but was constant during a day. No efforts were made to modify instrument optical parameters on a day-to-day basis to control a.

The LA-MC-ICPMS technique followed a published method (*36*), in which single-spot analyses were made using a 30 μm diameter beam size with an energy density of ~9–10 J cm^{-2}. Standard-sample bracketing was used to correct for the instrumental mass bias of unknown pyrite samples using standard-solutions calibrated against in-house pyrite standards of known composition (GAV-18=10.4‰; ALV-4053=2.5‰).
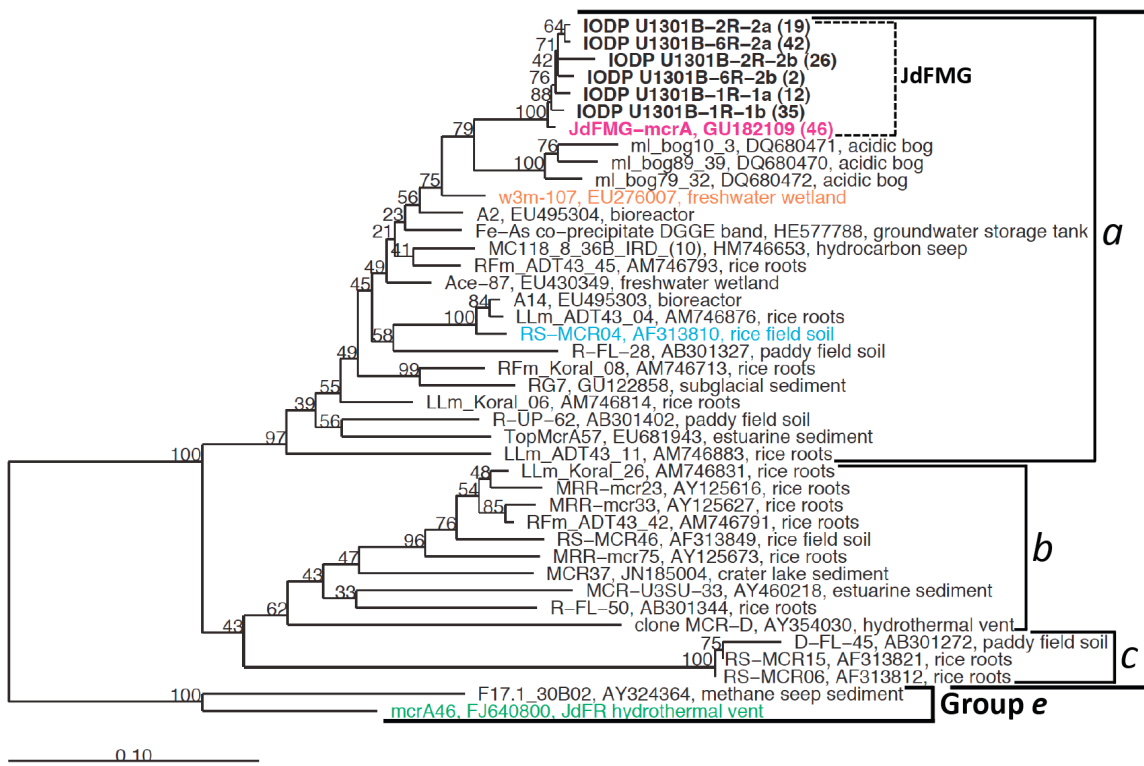
Solid-phase C Analyses. TOC content was determined by element analyzer (EA). Traces of carbonate C were removed by reaction with dilute (3N) HCl, followed by washing in distilled H_2O (*37*). $\delta^{13}C$-TOC was determined with a Costech EA coupled to a Thermo Scientific Delta V plus isotope ratio MS (IRMS), using IAEA 600 Caffeine ($\delta^{13}C$ = -27.77‰ VPDB) and IAEA-CH-6 Sucrose (-10.45‰) as calibration standards. Rock powders were degassed at 100˚C and stored under vacuum to minimize adsorption of atmospheric CO_2. Replicate analyses of low-C content samples (<500 ppm) were within ± 70 ppm and ± 0.5‰ $\delta^{13}C$. C blanks are less than 6% of reported C contents. $\delta^{13}C$-carbonate was analyzed as described previously (*10*). Since the carbonate content of rocks used for bulk geochemical analyses and smectite-dominated veins used for genetic analyses was too low for $\delta^{13}C$-analyses, carbonate-dominated major veins were used.

Basalt enrichments. Methanogen Medium 141 (Deutsche Sammlung von Mikroorganismen und Zellkulturen) was prepared with minor modifications (Table S8). The initial inoculum consisted of fresh basalt shards from rock interiors in which drilling fluid contamination was near or below the detection limit (<0.1 contaminant cells g^{-1} basalt; 1R-1-79, 14R-1-11, 23R-2-21) (*31*). For transfers, a few incubated basalt pieces were added to fresh medium containing triple-autoclaved basalt pieces and no sulfate. Headspace methane and dissolved species (sulfate, sulfide, DIC) were measured via standard protocols. $\delta^{13}C$-methane was determined using a Trace GC coupled via GC combustion III interface to a Delta plus XP plus IRMS (all Thermo Finnigan) following a previously published protocol (*38*). The absence of color changes due to oxidation of resazurin indicated that media remained fully anoxic throughout incubations.
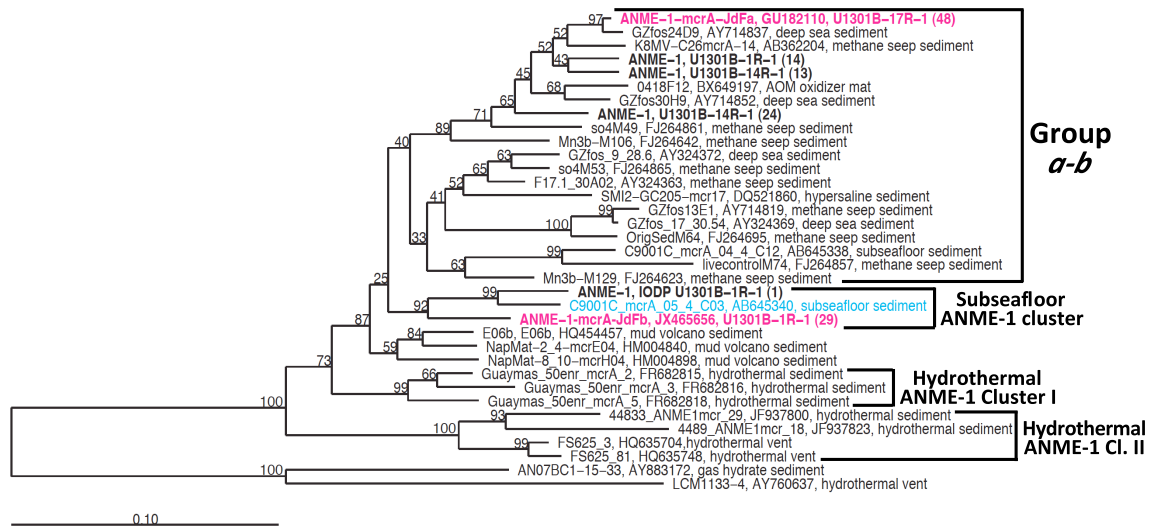
Figure S1. (A) Map of study area. (B) General direction of subsurface flow from Grizzly Bare outcrop to the Baby Bare Spring area and U1301 (*6, 11*). (C) Cross section through basalt core from U1301B, showing the alteration halos that surround basalt veins or fractures (adapted from (*9*)).
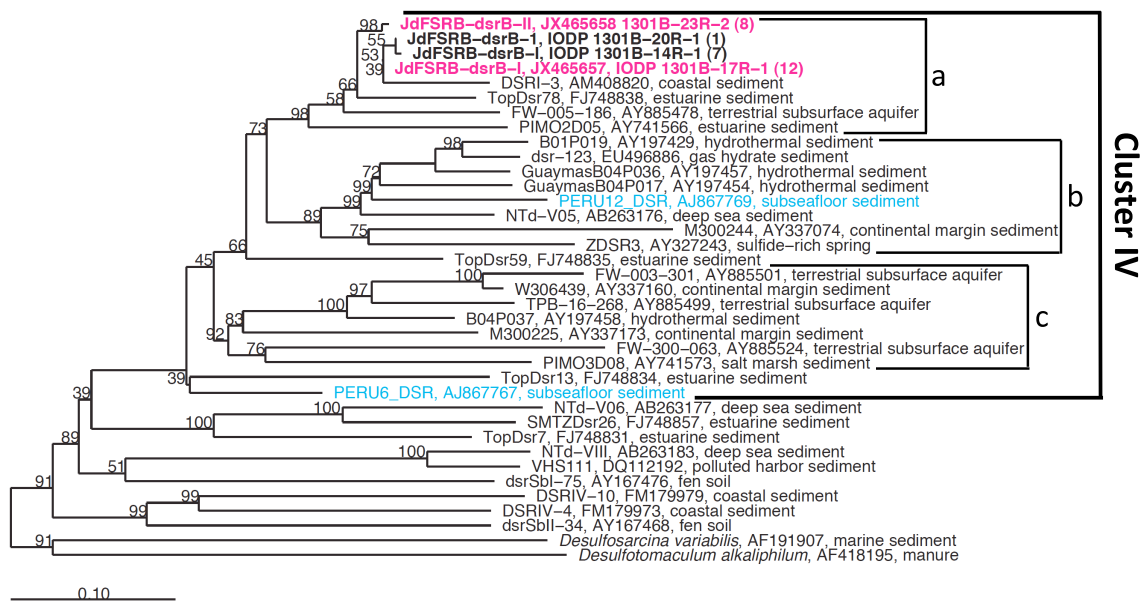
Figure S2. Phylogenetic tree of the Uncultivated Methanosarcinales Cluster (congruent with the Unidentified Rice Field Soil mcrA (*15*) and Zoige cluster I (ZC-I); *16*) based on *mcrA* nucleic acid sequences. The uncultivated Methanosarcinales group *e* is used as an outgroup. All phylotypes detected in this study in bold type face, with the one displayed in Fig. 1a in magenta. Clone numbers sequenced for each phylotype are shown in parentheses. The closely related methanogenic phylotype that was enriched in wetland sediment is in orange (*16*), the closest relative of an *mcrA* gene detected in Juan de Fuca Ridge seafloor basalt by microarray analysis appears in blue (*18*), and the closest relative from Juan de Fuca Ridge hydrothermal vent chimneys in green (*17*). The phylogeny was inferred using ARB Neighbour Joining, with Jukes-Cantor correction. Bootstrap support (in %, 1,000 replications) is indicated at each branching point.
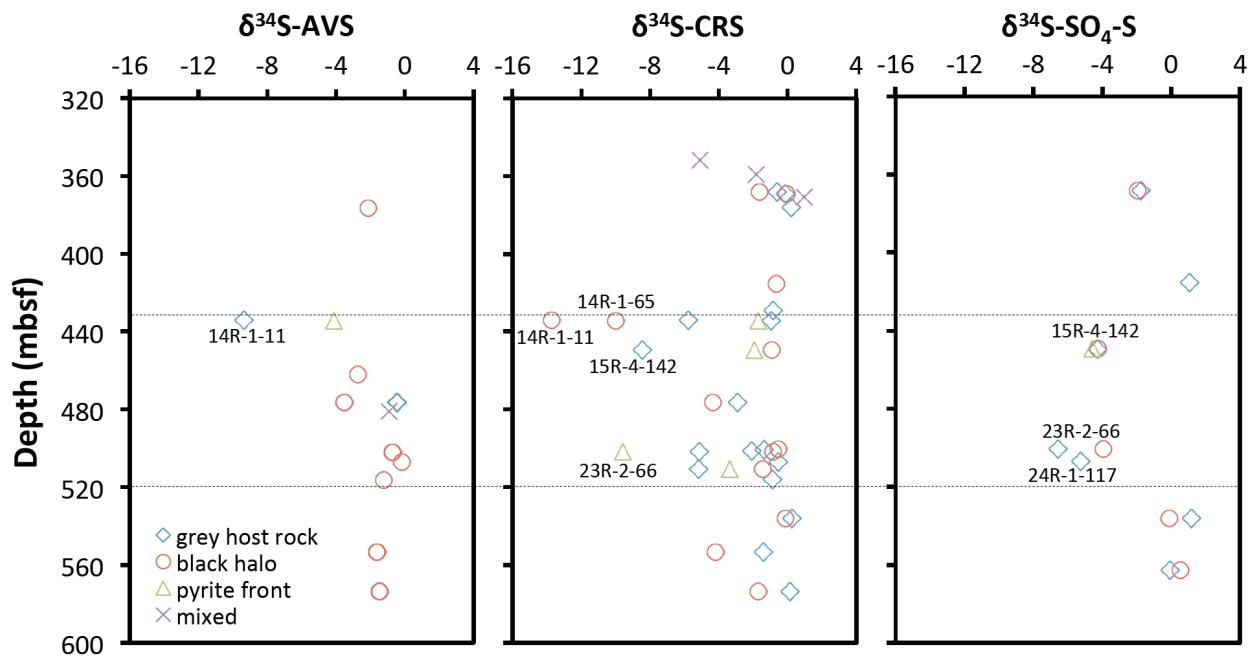
Figure S3. Phylogenetic tree of ANME-1 based on *mcrA* nucleic acid sequences. All phylotypes from subseafloor basalt of the Juan de Fuca Ridge Flank in bold type face, with ones included in Fig. 1A in magenta. Clone numbers sequenced for each phylotype are shown in parentheses. Highlighted in cyan is the only other deep subseafloor ANME-1 sequence in Genbank, from sediments of the Northwest Pacific off Shimokita Peninsula (Nunoura et al., unpubl.). Highly divergent ANME-1 sequences from the Lost City Hydrothermal Field (LCM1133-4) and gas hydrate sediment (AN07BC1-15-33) form a distinct cluster of their own, and are used as an outgroup. The phylogeny was inferred using ARB Neighbour Joining, with Jukes-Cantor correction. Bootstrap support (in %, 1,000 replications) is indicated at each branching point.
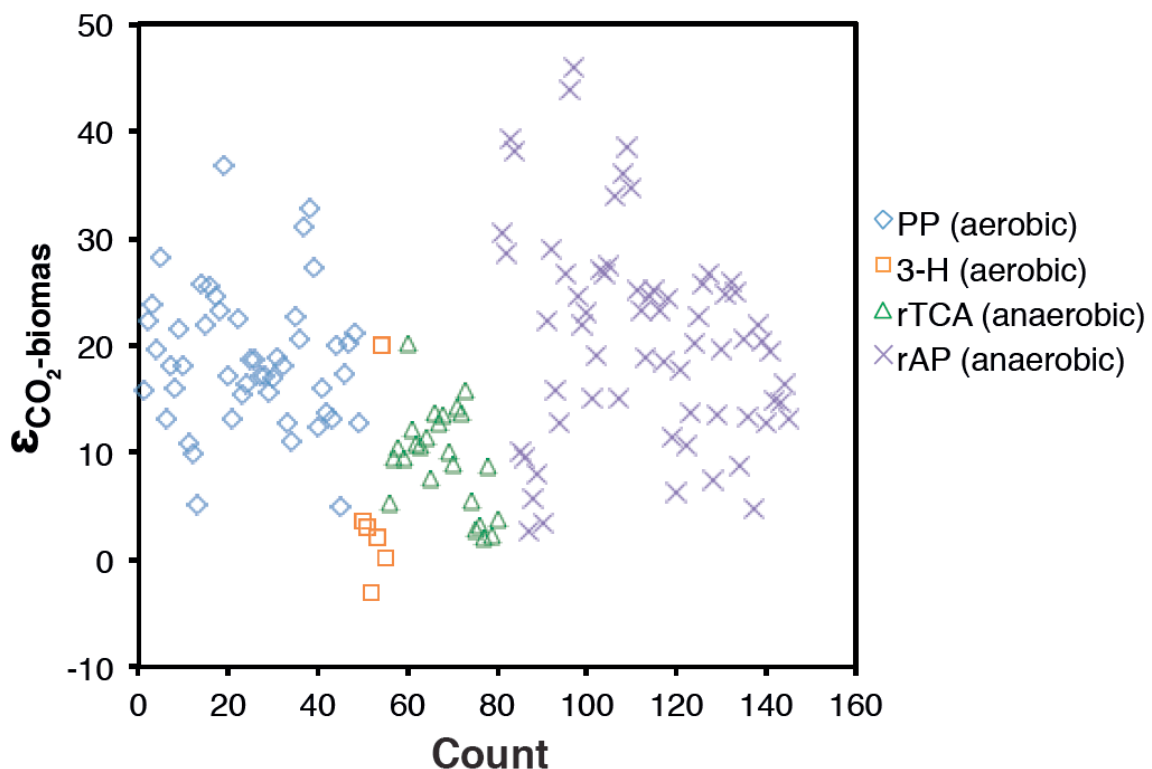
Figure S4. Phylogenetic tree of Cluster IV and related *dsrB* clusters, based on nucleic acid sequences. Phylotypes from Juan de Fuca Ridge Flank basalt appear in bold type face, with ones shown in Fig. 1B in magenta. Clone numbers sequenced for each phylotype are shown in parentheses. Sequences detected in subsurface sediment of the Peru Margin are shown in blue (*21*). Cluster IV falls into at least 3 distinct subclusters (*a-c*) that each have high bootstrap support (>85%). All JdFSRG fall into subcluster *a*. The phylogeny was inferred using ARB Neighbour Joining with Jukes-Cantor correction. Sequences of Desulfobacteraceae (*Desulfosarcina variabilis*) and Firmicutes (*Desulfotomaculum alkaliphilum*) used as outgroups. Bootstrap support (in %, 1,000 replicates) shown at each branching point.
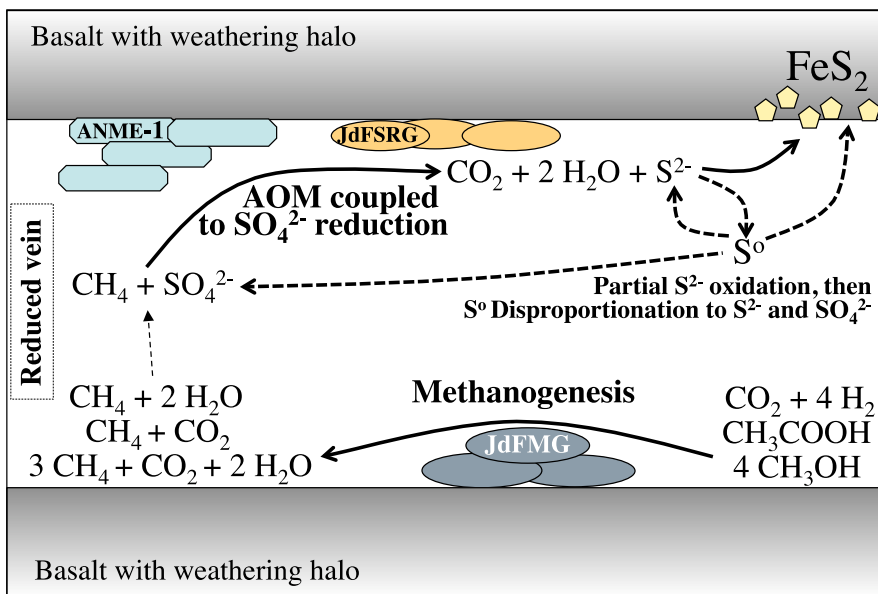
Figure S5. (A) Relative weight contributions of AVS, CRS, and SO$_4$-S to total S; (B) Cumulative weight contributions of AVS, CRS, and SO$_4$-S to total basalt sample. Sample IDs are shown in the middle. Rock samples in which DNA extracts were tested for *dsrB* presence are indicated on the far left. All data is listed in Table S2. B = black alteration halo; G = grey host rock; P = pyrite front, a narrow zone (typically <0.1mm) of concentrated disseminated pyrite along the boundary between an alteration halo and the adjacent host rock, located at interface of black alteration halo and grey host rock; M = mixed lithology.
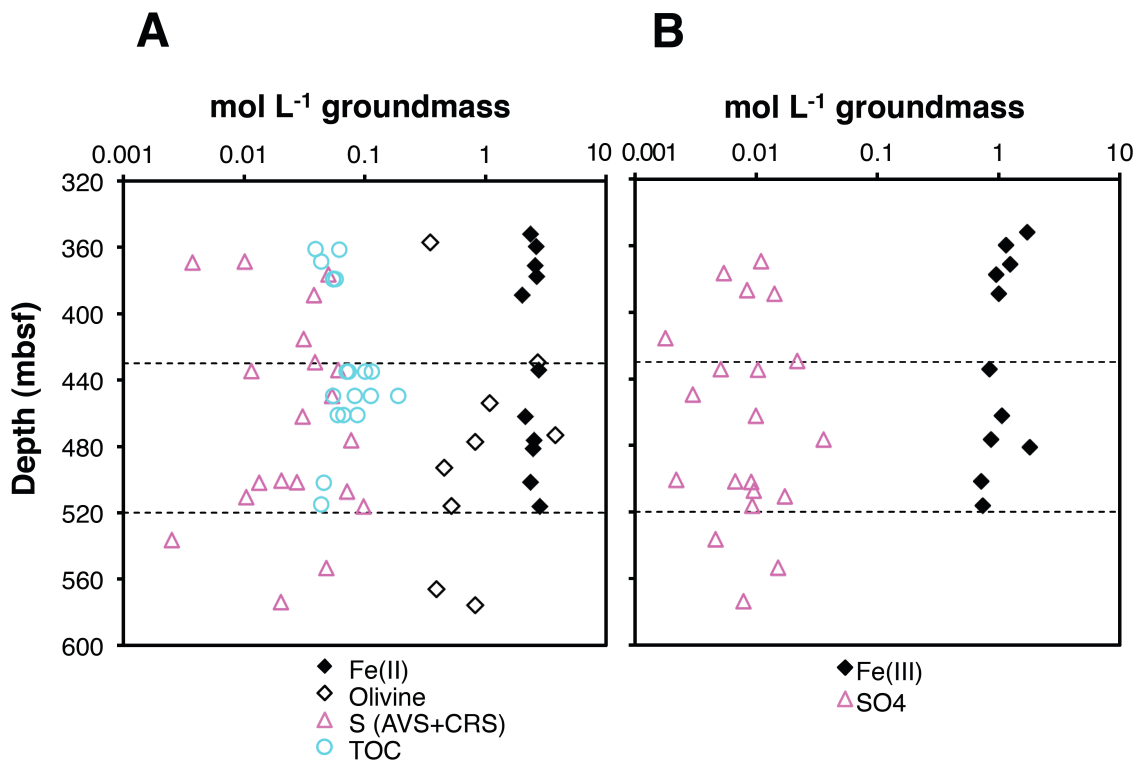
Figure S6. Depth-related trends in δ^{34}S of CRS, AVS, and SO$_4$-S at IODP Site U1301. The more reduced intermediate depth interval falls between the dashed lines. All δ^{34}S-values are expressed in ‰ vs. VCDT.

Figure S7. Compiled data from Table S6 on δ^{13}C-fractionations associated with aerobic and anaerobic C-fixation pathways. Abbreviations: PP = pentose phosphate (Calvin-Benson-Bassham) cycle, 3-H = 3-hydroxypropionate cycle, rTCA = reverse tricarboxylic acid cycle, rAP = reductive acetyl CoA pathway. Note that the PP pathway also occurs in some anoxygenic phototrophs (*Chromatium*, *Thiocapsa*, *Rhodospirillum*; Table S6).

Figure S8. Concept sketch of microbial methane and S-cycling in reduced veins of Juan de Fuca subsurface basalt (e.g. core 17R-1-70). Potential methanogenic substrates include H_2/CO_2, acetate, and methylated organic substrates. Methanogens, methanotrophs and sulfate reducers may coexist (as shown) or inhabit separate chemical microenvironments.

Figure S9. (A) Molar contents of the potential electron donors Fe(II), reduced S (includes both AVS- and CRS-S), and TOC per liter of basalt groundmass in borehole U1301B. Values for Fe(II) in olivine ((Mg, Fe)$_2$SiO$_4$) are also shown. (B) Molar contents of the potential electron acceptors Fe(III) and SO$_4$ per liter of groundmass at U1301B. The more reduced intermediate depth interval falls between the dashed lines. Except for olivine, which was obtained from Fisher et al. (2005; *9*), all data from this study. See Table S10 for a listing of potential energy-yielding reactions in borehole U1301.

Table S1. Sample identity, depth, lithology, total S and TOC content in host rock and halos (n=sample size), Fe(II) fraction of total Fe (FeT), δ^{34}S-pyrite, δ^{34}S-CRS and -AVS of host rock[1] and halos[1] (halos in parentheses), δ^{13}C-TOC, *mcrA* and *dsrB* clone library composition with number of clones obtained for each phylotype in parentheses. [wt% = % of sample weight, bd = below detection; nd = not determined; δ^{13}C-values in ‰ vs. Vienna Pee Dee Belemnite (VPDB), δ^{34}S in ‰ vs. Vienna-Canyon Diablo Troilite (VCDT)].

Sample ID[2]	Depth (mbsf)	Lithology[3]	Total S (wt%)[4]	TOC (wt%)	Fe^{3+}/FeT[5]	δ^{34}S (‰) pyrite (‰)	CRS (‰)[6]	AVS (‰)[6]	δ^{13}C-TOC (‰)	*mcrA* cluster (# of clones)	*dsrB* cluster (# of clones)
1R-1-79	352.0	20% breccia and pillow basalt (30% black halo) with small disseminated sulfide grains	0.04	nd	0.42	bd	-5.1	nd	nd	JdFMG (47), ANME-1 (44)	nd
2R-2-98	359.6	pillow basalt, brown/black halos (80%)	0.06	0.017-0.027 (n=3)[6]	0.30	bd	-1.8	nd	-21.6 to -26.6 (n=3)[7]	JdFMG (45)	nd
4R-4-7	371.2	pillow basalt, brown halo (Fe oxides)	0.05	0.019 (halo 0.025)[6]	0.32	bd	1	nd	-34.6 (halo -34.0)[7]	bd	nd
5R-1-22	377.5	pillow basalt, close to pillow rim	0.09	0.024-0.025 (n=4)[6]	0.26	bd	0.2	-2.1	-32.0 to -32.8 (n=4)[7]	bd	bd
6R-2-129	388.8	pillow basalt with black halo	0.07 (halo 0.03)	nd	0.33 (halo 0.47)	bd	-2.7	nd	nd	JdFMG (44)	nd
14R-1-11	434.1	massive basalt with black halo (pyrite disseminated in groundmass)	0.12 (halo 0.10)	0.031-0.050 (n=4)	0.23 (halo 0.38)	-4 to -47	-5.7 (-13.7)	(-9.3)	-21.9 to -26.5 (n=4)	ANME-1 (37)	Group IV (7)
17R-1-70	462.1	pillow basalt with black halo, pyrite in groundmass and along veins	0.10 (halo 0.04)	0.026-0.038 (n=3)	0.33 (halo 0.41)	-35 to -72	nd	-2.7	-26.0 to -27.6 (n=3)	JdFMG (46), ANME-1 (48)	Group IV (12)
20R-1-57	481.2	pillow basalt with oxidized groundmass (no pyrite)	0.03	nd	0.42	bd	nd	-0.9	nd	bd	Group IV (1)
23R-2-21	501.6	pillow basalt with black halo, only a single pyrite crystal found; brown halo	0.05 (halo 0.07)	0.020	0.23 (halo 0.24)	-2 to -3	-2.1	0.0 (0.0)	-33.5	bd	Group IV (8)
26R-1-76	516.3	pillow basalt with black halo, no pyrite found	0.13 (halo 0.08)	0.019	0.21 (halo 0.28)	bd	-0.9	-1.22	-33.9	bd	bd

[1] host rock = main basalt type; exhibits a pervasive dark gray background alteration manifest by secondary saponite; halo = distinctly colored band of rock (typically 1-15mm wide) flanking a vein; color imparted by differing secondary minerals (black halos contain celadonite, brown halos contain iron oxy-hydroxide)

[2] Sample designation as follows: 1R-1-79 = core 1, sampled by Rotary Core Barrel (R), section 1, 79 cm from section top

[3] from (*9*)

[4] total S determined by elemental analyzer

[5] Fe^{2+} determined by titration, total Fe (FeT) by Inductively Coupled Plasma Atomic Emission Spectroscopy (ICP-AES), Fe^{3+} calculated from difference.

[6] only samples with detectable CRS or AVS were analyzed

[7] values from within the same core, but not from the same rock used for genetic analyses (Table S3)

Table S2. Solid-phase S weight % (wt %) of basalt (wt %), relative contributions of different S pools to total S (%), and δ^{34}S of these same S pools. Bold font indicates samples also used for DNA extractions [bd = below detection; - = not determined; δ^{34}S in ‰ vs. VCDT.]

	Depth	S pools (wt %)				% contributions			δ^{34}S		
	mbsf	AVS	CRS	SO$_4$-S	Total	AVS	CRS	SO$_4$-S	AVS	CRS	SO$_4$-S
1R-1-79M	**352.0**	**0.00**	**0.05**	**0.01**	**0.05**	**0**	**84**	**16**	**bd**	**-5.1**	**-**
2R-2-98M	**359.6**	**0.00**	**0.04**	**0.01**	**0.05**	**2**	**87**	**12**	**bd**	**-1.8**	**-**
4R2-45B	368.5	0.00	0.03	0.01	0.04	2	77	21	bd	-1.6	-1.9
4R2-45G	368.5	0.00	0.01	0.00	0.01	6	86	8	bd	-0.6	-1.7
4R-2-122B	369.3	0.00	0.04	0.01	0.04	1	83	17	bd	-0.1	-
4R-2-122G	369.3	0.00	0.01	0.01	0.02	0	37	63	bd	-0.1	-
4R-2-122P	369.3	0.00	0.00	0.01	0.02	1	25	74	bd	bd	-
4R-4-7M	**371.2**	**0.00**	**0.00**	**0.01**	**0.01**	**0**	**5**	**95**	**bd**	**1.0**	**-**
5R-1-22G	**376.5**	**0.02**	**0.05**	**0.01**	**0.07**	**25**	**66**	**10**	**-2.1**	**0.2**	**-**
6R-1-72B	386.7	0.00	0.00	0.00	0.01	0	21	79	bd	bd	-
6R-1-72G	386.7	0.00	0.00	0.01	0.01	0	0	100	bd	bd	-
6R-2-129B	**388.8**	**0.00**	**0.00**	**0.01**	**0.01**	**0**	**15**	**85**	**bd**	**bd**	**-**
6R-2-129G	**388.8**	**0.00**	**0.05**	**0.02**	**0.06**	**0**	**73**	**27**	**bd**	**-2.7**	**-**
10R1-65B	415.5	0.00	0.00	0.00	0.00	0	89	11	bd	-0.7	bd
10R1-65G	415.5	0.00	0.04	0.00	0.04	0	95	5	bd	bd	1.1
12R-1-28G	429.2	0.00	0.05	0.03	0.07	0	64	36	bd	-0.8	-
14R-1-11B	**434.1**	**0.02**	**0.00**	**0.01**	**0.03**	**67**	**12**	**21**	**-9.3**	**-13.7**	**-**
14R-1-11G	**434.1**	**0.00**	**0.07**	**0.01**	**0.08**	**0**	**92**	**8**	**bd**	**-5.7**	**-**
14R-1-65B	434.7	0.00	0.03	0.01	0.05	0	75	25	bd	-9.9	-
14R-1-65G	434.7	0.00	0.01	0.01	0.03	0	53	47	bd	-0.9	-
14R-1-65P	434.7	0.04	0.38	0.01	0.44	10	87	3	-4.1	-1.7	-
15R4-142B	449.5	0.00	0.00	0.01	0.01	0	37	63	bd	-0.9	-4.2
15R4-142G	449.5	0.00	0.07	0.00	0.07	0	95	5	bd	-8.4	-4.3
15R4-142P	449.5	0.00	0.37	0.00	0.37	0	99	1	bd	-1.9	-4.6
17R-1-70G	**462.1**	**0.04**	**0.00**	**0.01**	**0.05**	**71**	**5**	**24**	**-2.7**	**bd**	**-**
19R-1-41B	476.5	0.01	0.01	0.01	0.02	26	30	44	-0.5	-4.4	-
19R-1-41G	476.5	0.02	0.08	0.04	0.14	11	57	32	-3.5	-2.9	-
20R-1-57M	**481.2**	**0.01**	**0.00**	**0.01**	**0.02**	**57**	**3**	**39**	**-0.9**	**bd**	**-**
23R1-66B	500.6	0.00	0.01	0.01	0.02	0	42	58	bd	-0.5	-3.9
23R1-66G	500.6	0.00	0.03	0.00	0.03	0	90	10	bd	-1.3	-6.5
23R-2-21G	**501.6**	**0.02**	**0.01**	**0.01**	**0.04**	**52**	**29**	**20**	**bd**	**-2.1**	**-**
23R-2-66B	502.0	0.00	0.00	0.00	0.01	21	49	31	bd	-0.8	-
23R-2-66G	502.0	0.01	0.01	0.01	0.03	26	33	40	-0.7	-5.1	-
23R-2-66P	502.0	0.00	0.03	0.01	0.04	6	61	33	bd	-9.6	-
24R1-117G	507.1	0.00	0.09	0.01	0.10	2	86	12	-0.2	-0.5	-5.2
25R-1-123B	510.7	0.00	0.01	0.00	0.01	14	48	38	bd	-1.5	-
25R-1-123G	510.7	0.00	0.01	0.02	0.03	10	27	62	bd	-5.2	-
25R-1-123P	510.7	0.00	0.02	0.01	0.03	12	61	27	bd	-3.4	-

26R-1-76G	**516.3**	**0.05**	**0.07**	**0.01**	**0.13**	**41**	**50**	**9**	**-1.2**	**-0.9**	**-**
30R1-119G	536.4	0.00	0.00	0.01	0.01	0	35	21	bd	0.3	1.2
30R1-119B	536.4	0.00	0.00	0.00	0.00	0	42	8	bd	-0.1	-0.1
32R-3-50B	553.4	0.00	0.01	0.01	0.01	1	54	45	bd	-4.2	-
32R-3-50G	553.4	0.03	0.03	0.02	0.08	34	42	24	-1.6	-1.4	-
34R2-82B	562.9	0.00	0.00	0.00	0.00	0	0	21	bd	bd	0.6
34R2-82G	562.9	0.00	0.00	0.00	0.00	0	0	8	bd	bd	0.0
36R-1-53B	573.7	0.00	0.01	0.00	0.01	0	68	32	bd	-1.7	-
36R-1-53G	573.7	0.01	0.02	0.01	0.03	21	51	28	-1.5	0.1	-

Table S3. Listing of individual $\delta^{34}S$ measurements by SIMS and laser ablation. In cases where only one measurement was made per granule, the $\delta^{34}S$-pyrite and mean $\delta^{34}S$ per pyrite granule are identical. All $\delta^{34}S$ are in ‰ versus VCDT. Samples in bold were also used for DNA extractions.

Analysis Type	Core ID	Depth (mbsf)	Granule ID	Granule Subsample ID	$\delta^{34}S$	Standard deviation	Mean $\delta^{34}S$
laser	13R-1	430.8	13	a	-46.4	0.2	-46.4
laser	13R-1	430.8	1	a	-40.5	0.3	-45.3
laser	13R-1	430.8	1	b	-51.3	0.2	
laser	13R-1	430.8	1	c	-45.3	0.2	
laser	13R-1	430.8	1	d	-32.2	0.2	
laser	13R-1	430.8	1	e	-50.6	0.3	
laser	13R-1	430.8	1	f	-51.0	0.3	
laser	13R-1	430.8	1	g	-46.0	0.3	
laser	13R-1	430.8	1	h	-45.3	0.2	
laser	13R-1	430.8	2	a	-2.4	0.2	-2.4
laser	13R-1	430.8	3	a	-3.9	0.2	-3.9
laser	13R-1	430.8	4	a	-3.4	0.2	-3.4
laser	13R-1	430.8	5	a	-3.4	0.2	-3.3
laser	13R-1	430.8	5	b	-3.4	0.3	
laser	13R-1	430.8	5	c	-3.1	0.2	
laser	13R-1	430.8	6	a	-3.4	0.2	-3.3
laser	13R-1	430.8	6	b	-3.2	0.2	
laser	13R-1	430.8	7	a	-3.5	0.2	-3.8
laser	13R-1	430.8	7	b	-4.2	0.2	
laser	13R-1	430.8	8	a	-3.9	0.2	-3.9
laser	13R-1	430.8	9	a	-3.7	0.2	-3.7
laser	13R-1	430.8	10	a	-4.6	0.2	-4.6
laser	13R-1	430.8	11	a	-5.6	0.2	-5.6
laser	13R-1	430.8	12	a	-5.9	0.2	-5.4
laser	13R-1	430.8	12	b	-5.2	0.2	
laser	13R-1	430.8	12	c	-5.1	0.2	
laser	**14R-1-11**	**434.7**	**1**	**a**	**-23.5**	**0.3**	**-25.8**
laser	**14R-1-11**	**434.7**	**1**	**b**	**-28.1**	**0.2**	
laser	**14R-1-11**	**434.7**	**2**	**a**	**-22.9**	**0.2**	**-21.7**
laser	**14R-1-11**	**434.7**	**2**	**b**	**-20.4**	**0.2**	
laser	**14R-1-11**	**434.7**	**3**	**a**	**0.4**	**0.2**	**0.3**
laser	**14R-1-11**	**434.7**	**3**	**b**	**0.8**	**0.2**	
laser	**14R-1-11**	**434.7**	**3**	**c**	**-0.2**	**0.2**	
laser	**14R-1-11**	**434.7**	**4**	**a**	**0.3**	**0.2**	**0.5**
laser	**14R-1-11**	**434.7**	**4**	**b**	**0.7**	**0.2**	
laser	**14R-1-11**	**434.7**	**5**	**a**	**-0.2**	**0.2**	**-0.2**
laser	**14R-1-11**	**434.7**	**6**	**a**	**-29.9**	**0.4**	**-32.2**
laser	**14R-1-11**	**434.7**	**6**	**b**	**-34.4**	**0.3**	

laser	**14R-1-11**	**434.7**	**7**	**a**	**-33.8**	**0.2**	**-35.2**
laser	**14R-1-11**	**434.7**	**7**	**b**	**-36.5**	**0.3**	
laser	**14R-1-11**	**434.7**	**8**	**a**	**0.4**	**0.2**	**0.7**
laser	**14R-1-11**	**434.7**	**8**	**b**	**1.1**	**0.2**	
laser	**14R-1-11**	**434.7**	**9**	**a**	**-46.6**	**0.2**	**-29.8**
laser	**14R-1-11**	**434.7**	**9**	**b**	**-13.0**	**0.2**	
laser	**14R-1-11**	**434.7**	**10**	**a**	**-7.7**	**0.2**	**-7.7**
laser	**14R-1-11**	**434.7**	**11**	**a**	**-4.9**	**0.2**	**-4.9**
laser	**14R-1-11**	**434.7**	**12**	**a**	**-8.7**	**0.3**	**-8.7**
laser	**14R-1-11**	**434.7**	**13**	**a**	**-9.0**	**0.3**	**-9.0**
sims	**14R-1-11**	**434.7**	**14**	**a**	**-10.4**	**0.5**	**-10.4**
sims	**14R-1-11**	**434.7**	**15**	**a**	**-3.3**	**0.7**	**-3.3**
sims	**14R-1-11**	**434.7**	**16**	**a**	**-19.4**	**0.6**	**-19.4**
laser	15R-2	445.9	1	a	-7.4	0.2	-7.2
laser	15R-2	445.9	1	b	-10.0	0.2	
laser	15R-2	445.9	1	c	-10.0	0.2	
laser	15R-2	445.9	1	d	-1.2	0.2	
laser	15R-2	445.9	2	a	-0.9	0.2	-0.9
laser	15R-2	445.9	3	a	-1.1	0.2	-1.1
laser	15R-2	445.9	4	a	-1.7	0.2	-1.7
laser	15R-2	445.9	5	a	-8.2	0.2	-8.2
laser	15R-2	445.9	6	a	-19.3	0.2	-19.3
laser	15R-2	445.9	7	a	-3.8	0.2	-8.6
laser	15R-2	445.9	7	b	-8.2	0.2	
laser	15R-2	445.9	7	c	-6.0	0.4	
laser	15R-2	445.9	7	d	-16.3	0.2	
laser	15R-2	445.9	8	a	-2.4	0.2	-2.4
laser	15R-2	445.9	9	a	-3.2	0.2	-3.2
laser	15R-2	445.9	10	a	-4.2	0.2	-4.2
laser	15R-2	445.9	11	a	-13.8	0.2	-13.8
laser	15R-2	445.9	12	a	-1.9	0.2	-1.9
laser	15R-2	445.9	13	a	-1.6	0.2	-1.6
laser	15R-2	445.9	14	a	-9.7	0.2	-9.7
sims	15R-2	445.9	1	a	-0.3	0.3	-0.3
sims	15R-2	445.9	2	a	-2.9	0.3	-2.9
sims	15R-2	445.9	3	a	-25.9	0.3	-25.9
sims	15R-2	445.9	4	a	-22.6	0.3	-22.6
sims	15R-2	445.9	5	a	-1.6	0.4	-1.6
sims	15R-2	445.9	6	a	-11.7	0.5	-11.7
sims	15R-2	445.9	7	a	-17.5	0.4	-17.5
sims	15R-2	445.9	8	a	-7.9	0.5	-7.9
sims	15R-2	445.9	9	a	-2.7	0.5	-2.7
sims	15R-2	445.9	10	a	-1.9	0.5	-1.9
sims	15R-2	445.9	11	a	-5.7	0.5	-5.7
laser	15R-4	449.5	1	a	-1.8	0.2	-1.8
laser	15R-4	449.5	1	b	-1.7	0.2	

laser	15R-4	449.5	2	a	-1.3	0.2	-1.3
laser	15R-4	449.5	3	a	-1.4	0.2	-1.5
laser	15R-4	449.5	3	b	-1.6	0.2	
laser	**17R-1-70**	**461.8**	**1**	**a**	**-65.1**	**0.2**	**-65.1**
laser	**17R-1-70**	**461.8**	**2**	**a**	**-69.0**	**0.2**	**-69.4**
laser	**17R-1-70**	**461.8**	**2**	**b**	**-70.1**	**0.2**	
laser	**17R-1-70**	**461.8**	**2**	**c**	**-69.4**	**0.2**	
laser	**17R-1-70**	**461.8**	**2**	**d**	**-69.0**	**0.2**	
laser	**17R-1-70**	**461.8**	**4**	**a**	**-63.4**	**0.3**	**-63.4**
laser	**17R-1-70**	**461.8**	**5**	**a**	**-68.5**	**0.2**	**-68.5**
laser	**17R-1-70**	**461.8**	**6**	**a**	**-35.2**	**0.2**	**-35.2**
sims	**17R-1-70**	**461.8**	**7**	**a**	**-70.4**	**0.4**	**-70.4**
sims	**17R-1-70**	**461.8**	**8**	**a**	**-72.4**	**0.4**	**-72.4**
sims	**17R-1-70**	**461.8**	**9**	**a**	**-71.2**	**0.5**	**-71.2**
sims	**17R-1-70**	**461.8**	**10**	**a**	**-71.5**	**0.3**	**-71.5**
sims	**17R-1-70**	**461.8**	**11**	**a**	**-58.6**	**0.4**	**-58.6**
laser	18R-2	473.1	1	a	-31.0	0.2	-30.1
laser	18R-2	473.1	1	b	-29.1	0.3	
laser	18R-2	473.1	2	a	-14.0	0.3	-9.9
laser	18R-2	473.1	2	b	-5.9	0.3	
laser	18R-2	473.1	3	a	-0.2	0.2	-13.1
laser	18R-2	473.1	3	b	-25.5	0.3	
laser	18R-2	473.1	3	c	-0.9	0.2	
laser	18R-2	473.1	3	d	-18.0	0.7	
laser	18R-2	473.1	3	e	-20.9	0.3	
laser	18R-2	473.1	4	a	-1.4	0.2	-4.9
laser	18R-2	473.1	4	b	-8.4	0.2	
laser	18R-2	473.1	5	a	-7.7	0.4	-3.5
laser	18R-2	473.1	5	b	0.8	0.2	
laser	18R-2	473.1	6	a	-15.9	0.2	-13.8
laser	18R-2	473.1	6	b	-11.8	0.2	
laser	18R-2	473.1	7	a	1.2	0.3	0.7
laser	18R-2	473.1	7	b	0.2	0.2	
laser	19R-1	476.5	2	a	-47.0	0.2	-47.8
laser	19R-1	476.5	2	b	-51.2	0.2	
laser	19R-1	476.5	2	c	-45.2	0.2	
laser	19R-1	476.5	3	a	-61.7	0.2	-62.5
laser	19R-1	476.5	3	b	-63.3	0.2	
laser	19R-1	476.5	4	a	-62.1	0.4	-62.1
laser	19R-1	476.5	5	a	-64.3	0.2	-64.3
laser	19R-1	476.5	6	a	-47.2	0.2	-47.2
sims	19R-1	476.5	7	a	-62.8	0.3	-62.8
sims	19R-1	476.5	8	a	-65.7	0.5	-65.7
sims	19R-1	476.5	9	a	-66.8	0.4	-66.8
sims	19R-1	476.5	10	a	-66.7	0.6	-66.7
sims	19R-1	476.5	11	a	-47.0	0.9	-47.0

sims	19R-1	476.5	12	a	-61.9	0.5	-61.9
sims	19R-1	476.5	13	a	-42.5	0.4	-42.5
laser	**23R-2-21**	**501.4**	**1**	**a**	**-2.7**	**0.2**	**-2.2**
laser	**23R-2-21**	**501.4**	**1**	**b**	**-1.6**	**0.2**	

Table S4. Summary of δ¹³C-TOC and TOC content data. *n* indicates the number of subsamples analyzed. Values of individual subsamples are indicated in italic, where more than 1 subsample was analyzed. δ¹³C-values are expressed in ‰ vs. VPDB, TOC content in wt. % of total basalt. [* = same sample also used for genetic analyses; - = not determined; G = grey host rock, B = Black halo.]

Core ID	*n*	Depth (mbsf)	δ¹³C (±SD)	Wt. %
2R-3-93	1	361.0	-21.6	-
2R-3-115	1	361.3	-26.6	0.017
2R-3-134	1	361.4	-23.7	0.027
4R-2-45B	1	368.6	-34.0	0.025
4R-2-45G	1	368.6	-34.6	0.019
5R-2-126 (mean)	4	379.1	-32.6 ± 0.4	0.024 (±0.001)
5R-2-126a			*-32.8*	*0.025*
5R-2-126b			*-32.8*	*0.024*
5R-2-126c			*-32.0*	*0.024*
5R-2-126d			*-32.8*	*0.024*
14R-1-11 (mean)*	4	434.1	-23.8 ± 2.0	0.039 (±0.009)
14R-1-11a			*-26.5*	*0.031*
14R-1-11b			*-24.0*	*0.032*
14R-1-11c			*-21.9*	*0.050*
14R-1-11d			*-22.6*	*0.044*
15R-4-142 (mean)	4	443.6	-27.9 ± 0.4	0.048 (±0.025)
15R-4-142a			*-28.4*	*0.024*
15R-4-142b			*-27.9*	*0.049*
15R-4-142c			*-27.9*	*0.036*
15R-4-142d			*-27.5*	*0.083*
17R-1-70 (mean)*	3	462.1	-26.9 ± 0.8	0.031 (±0.006)
17R-1-70a			*-27.6*	*0.026*
17R-1-70b			*-27.2*	*0.029*
17R-1-70c			*-26.0*	*0.038*
23R-2-21*	1	499.9	-33.5	0.020
26R-1-76*	1	515.5	-33.9	0.019

Table S5. Overview of δ^{13}C-carbonate values. All measurements expressed in ‰ vs. VPDB.

Sample	Depth (mbsf)	δ^{13}C
5R-3-47	379.8	0.06
12R-1-28	429.2	-1.78
18R-2-27	472.6	-5.07
18R-2-34	472.6	-4.68
18R-2-55	472.9	-4.06
18R-3-16	473.7	-3.87
18R-3-49	474.1	-2.80
18R-3-88	474.4	-3.36
18R-3-106	474.6	-3.49
18R-3-118	474.7	-1.74
18R-4-0	474.9	-2.97
18R-4-9	475.0	-3.94
35R-2-49	565.6	-1.78

Table S6. Compilation of δ^{13}C-isotopic fractionations from carbon dioxide (CO_2) to cell biomass across known C-fixation pathways. Data compiled from seven different studies (*26, 39-44*) and references within. All data from pure cultures except where marked with an asterisk - asterisks indicate measurements on natural samples. Pathway means and standard deviations were determined on strain averages, where more than one published value was available. PP = pentose phosphate cycle (Calvin Benson Bassham Cycle), 3-H = 3-hydroxypropionate cycle, rTCA = reverse tricarboxylic acid cycle, rAP = reductive acetyl CoA pathway, ε_{CO2} to cells = C-isotopic fractionation from CO_2 to cell biomass, N/A = not applicable.

Count	Path-way	Organism	T_{growth} (°C)	$\varepsilon_{CO2-cell}$ strain (‰)	strain mean (‰)	strain SD (‰)	Ref.
1	PP	*Agmenellum quadrupicatum*	39	15.9	20.4	3.5	26
2	PP	" "	39	22.2			26
3	PP	" "	39	23.9			26
4	PP	" "	39	19.6			26
5	PP	*Alkaligenes eutrophus*	28	28.2	28.2		26
6	PP	*Anacystis nidulans*	39	13.1	17.3	3.1	26
7	PP	" "	39	18			26
8	PP	" "	33	16			26
9	PP	" "	33	21.5			26
10	PP	" "	33	18			26
11	PP	*Rhodopseudomonas capsulata*		10.8	10.4		26
12	PP	" "	30	9.9			26
13	PP	*Thiobacillus novellus**	30	5.1	5.1		39
14	PP	*Thiobacillus neapolitanus**		25.8	25.8		26
15	PP	*Thiocapsa roseopersicina**	28	22	22.0		26
16	PP	*Thiomicrospira* sp. L-12*		25.5	25.5		26
17	PP	*Thiomicrospira crunogena**		24.5	24.5		26
18	PP	*Thiomicrospira crunogena**		23.3	23.3		26
19	PP	*Chlamydomonas reinhardtii**	20	36.8	36.8		26
20	PP	*Microcoleus chthonoplastes*	39	17.1	17.1		26
21	PP	*Schizothrix calcicola*	39	13.2	13.2		26
22	PP	*Synechococcus* sp.	57	22.5	17.8	2.0	26
23	PP	" "		15.5			26
24	PP	" "		16.4			26
25	PP	" "		18.6			26
26	PP	" "		18.6			26
27	PP	" "		17.2			26

28	PP	" "		17.1			26
29	PP	" "		15.6			26
30	PP	" "		16.9			26
31	PP	" "		18.9			26
32	PP	" "		18.1			26
33	PP	*Synechococcus lividus*	47	12.8	12.0		26
34	PP	" "	70	11.1			26
35	PP	*Chlorella sorokiniana*	39	22.6	22.6		26
36	PP	*Chromatium tepidum*	50	20.5	20.5		26
37	PP	*Chromatium* strain D*	20	31	31.9		26
38	PP	" " *	20	32.7			26
39	PP	*Chromatium vinosum**	20	27.3	27.3		26
40	PP	*Coccochloris elebens*	39	12.3	14.2		26
41	PP	" "	39	16			26
42	PP	*Nitrosomonas europaea**		13.8	15.7	3.8	26
43	PP	" " *		13.2			26
44	PP	" "		20			40
45	PP	*Oscillatoria williamsii*	39	5	11.2		26
46	PP	" "	39	17.3			26
47	PP	*Oscillochloris trichoides**	28	20.1	20.1		26
48	PP	*Rhodospirillum rubrum*	20	21.1	16.9		26
49	PP	" "	20	12.7			26
50	3-H	*Acidianus brierleyi*	65	3.6	3.6		39
51	3-H	*Metallosphaera sedula*	65	3.1	0.7	3.3	39
52	3-H	" "	65	-3			26
53	3-H	" " *	65	2			26
54	3-H	*Nitrosopumilus maritimus*		20	20.0		41
55	3-H	*Sulfolobus solfataricus*	85	0.2	0.2		39
56	rTCA	*Aquifex aeolicus*	85	5.4	5.4		39
57	rTCA	*Chlorobium limicola*	30	9.5	9.5		26
58	rTCA	*Chlorobium phaeovibrioides**	30	10.4	10.0		26
59	rTCA	" " *	30	9.5			39
60	rTCA	*Chlorobium thiosulfatophilum**	20	20.1	20.1		26
61	rTCA	*Chlorobium vibrioforme**	30	12.2	11.3	0.7	26
62	rTCA	" "	30	10.8			39
63	rTCA	" "	30	10.7			26
64	rTCA	" "	28	11.4			26
65	rTCA	*Chloroflexus aurantiacus*	55	7.6	11.9	2.9	39
66	rTCA	" " *	55	13.7			39
67	rTCA	" "	55	12.7			26
68	rTCA	" "	55	13.6			26
69	rTCA	*Desulfobacter hydrogenophilus*	28	10	12.5	3.0	39
70	rTCA	" "	28	8.9			39

71	rTCA	"	"	28	14.2			39
72	rTCA	"	"	28	13.7			42
73	rTCA	"	"	30	15.9			43
74	rTCA	*Hydrogenobacter thermophilus*		70	5.5	5.5		39
75	rTCA	*Pyrobaculum aerophilum*		100	2.9	2.9		39
76	rTCA	*Thermocrinis ruber*		85	3.3	3.3		26
77	rTCA	*Thermoproteus neutrophilus*		85	2	5.4		39
78	rTCA	"	"		8.7			26
79	rTCA	*Pyrodictium occultum*		102	2.3	2.3		39
80	rTCA	*Pyrolobus fumarii*		105	3.8	3.8		39
81	rAP	*Desulfotomaculum acetoxidans*		30	30.5	29.5		42
82	rAP	"	"	30	28.5			43
83	rAP	*Desulfobacterium autotrophicum*		28	39.3	24.3	16.7	26
84	rAP	"	"	28	38.2			26
85	rAP	"	"	30	10			42
86	rAP	"	"		9.6			43
87	rAP	*Archaeoglobus fulgidus*		85	2.7	4.3		39
88	rAP	"	"	85	5.8			39
89	rAP	*Archaeoglobus lithotrophicus*		85	8	8.0		39
90	rAP	*Ferroglobus placidus*		85	3.5	3.5		39
91	rAP	*Acetobacterium woodii*		28	22.2	22.3	6.6	26
92	rAP	"	"	28	29			26
93	rAP	"	"	28	15.8			26
94	rAP	M.*bacterium thermoautotrophicum*		65	12.7	25.9	9.9	44
95	rAP	"	"	65	26.6			44
96	rAP	"	"	65	43.8			44
97	rAP	"	"	65	46			44
98	rAP	"	"	65	24.5			44
99	rAP	"	"	65	21.9			44
100	rAP	"	"	65	23.1			44
101	rAP	"	"	65	15			39
102	rAP	"	"	65	19.1			26
103	rAP	"	"	56	27			44
104	rAP	"	"	56	26.6			44
105	rAP	"	"	66	27.4			44
106	rAP	"	"		34			44
107	rAP	"	"	65	15			39
108	rAP	*Methanobacterium formicicum*		34	36.1	36.4	1.9	44
109	rAP	"	"	34	38.4			44
110	rAP	"	"	34	34.7			44
111	rAP	*Methanobacterium* sp.		37	25.1	22.9	2.8	26
112	rAP	"	"	37	23.2			26
113	rAP	"	"	46	18.8			26

114	rAP	" "	46	24.5			26
115	rAP	M.*bacterium* sp. strain Ivanov	37	25.2	22.8	3.0	44
116	rAP	" "	37	23.2			44
117	rAP	" "	46	18.5			44
118	rAP	" "	46	24.3			44
119	rAP	M.*bacterium* strain M.o.H.	40	11.5	11.5		44
120	rAP	M.*caldococcus jannaschii*	85	6.2	12.1	4.9	39
121	rAP	" "	85	17.7			39
122	rAP	" "	85	10.7			39
123	rAP	" "	85	13.7			39
124	rAP	*Methanococcus igneus*	85	20.2	21.5		39
125	rAP	M.*coccus thermolithotrophicus*	65	22.7	18.6	7.6	39
126	rAP	" "	65	25.8			39
127	rAP	" "	65	26.7			39
128	rAP	" "	41	7.4			39
129	rAP	" "	51	13.5			39
130	rAP	" "	60	19.7			39
131	rAP	" "	65	24.8			39
132	rAP	" "	65	26			39
133	rAP	" "	70	24.9			39
134	rAP	" "	65	8.7			39
135	rAP	" "	45	20.5			39
136	rAP	" "	45	13.4			39
137	rAP	" "	45	4.8			39
138	rAP	" "	65	22			39
139	rAP	*Methanopyrus kandleri*	100	20.3	16.5		39
140	rAP	" "	100	12.7			39
141	rAP	*Methanosarcina barkeri*	37	19.5	16.3	2.3	39
142	rAP	" "	40	14.8			44
143	rAP	" "	37	14.6			44
144	rAP	" "	37	16.3			44
145	rAP	*Methanothermus fervidus*	85	13.1	13.1		39

Table S7. Mean δ^{13}C-isotopic fractionations from CO_2 to cell biomass ($\varepsilon_{CO2\text{-}cells}$) in microbes using the reductive acetyl CoA pathway, calculated from compiled data in table S6.

Taxon	Energy metabolism	$\varepsilon_{CO2\text{-}cells}$ (‰) mean	SD	Ref.
Desulfotomaculum acetoxidans	SO_4^{2-} reducer, H_2/CO_2	29.5		*42-43*
Desulfobacterium autotrophicum	SO_4^{2-} reducer, H_2/CO_2	24.3	16.7	*26, 42-43*
Archaeoglobus fulgidus	SO_4^{2-} reducer, H_2/CO_2	4.3		*39*
Archaeoglobus lithotrophicus	SO_4^{2-} reducer, H_2/CO_2	8.0		*39*
Ferroglobus placidus	Fe^{3+}, NO_3^-, $S_2O_3^{2-}$ reducer	3.5		*39*
Acetobacterium woodii	acetogenesis, H_2/CO_2	22.3	6.6	*26, 42-43*
M.bacterium thermoautotrophicum	methanogenesis, H_2/CO_2	25.9	9.9	*26, 39, 44*
Methanobacterium formicicum	methanogenesis, H_2/CO_2	36.4	1.9	*44*
Methanobacterium sp.	methanogenesis, H_2/CO_2	22.9	2.8	*26*
Methanobacterium sp. strain Ivanov	methanogenesis, H_2/CO_2	22.8	3.0	*44*
Methanobacterium strain M.o.H.	methanogenesis, H_2/CO_2	11.5		*44*
Methanocaldococcus jannaschii	methanogenesis, H_2/CO_2	12.1	4.9	*39*
Methanococcus igneus	methanogenesis, H_2/CO_2	21.5		*39*

Table S8. Media composition for initial enrichment and transfer. The composition, including the trace element and vitamin solutions, follows the methanogenic Medium 141 (DSMZ) except where indicated in bold. 2 atm headspace pressure of 80% H_2: 20% CO_2 were applied. The final pH was adjusted to 8.0. All incubations were at 65°C.

Ingredients of Medium	Initial Enrichment Quantity L^{-1}	Transfer Quantity L^{-1}
KCl	0.34 g	0.34 g
$MgCl_2$ x 6 H_2O	4.0 g	6.85 g
$MgSO_4$ x 7 H_2O	3.45 g	omitted
NH_4Cl	0.25 g	0.25 g
$CaCl_2$ x 2 H_2O	0.14 g	0.14 g
K_2HPO_4	0.14 g	0.14 g
NaCl	18.0 g	18.0 g
$Fe(NH_4)_2(SO_4)_2$ x 7 H_2O	2 mg	2 mg
$NaHCO_3$	2.5 g (29.8 mM)	2.500 g (29.8 mM)
Na-acetate	0.082 g (1 mM)	0.164 g (2 mM)
Methanol stock (300 mM)	0.17 mL (50 µM)	1 mL (300 µM)
Dimethyl sulfide stock (30 mM)	1.67 mL (50 µM)	10 mL (300 µM)
Yeast extract (Difco)	0.20 g	0.200 g
Trypticase (BBL)	2.00 g	2.00 g
Resazurin	1 mg	1 mg
Cysteine-HCl x H_2O	0.50 g	0.50 g
Na_2S x 9 H_2O	0.50 g	0.50 g
Trace elements	10 mL	10 mL
Vitamin solution	10 mL	10 mL
Distilled water, added to:	1000 mL	1000 mL

Table S9. Basalt media composition after 7 years (initial) and 5 years (1st transfer) of incubation. bd = below detection; δ^{13}C-values in ‰ vs. VPDB.

Core ID	Replicate	enrichment	CH$_4$ (μM)	SO$_4^{2-}$ (mM)[1]	H$_2$S (mM)[2]	DIC (mM)[3]	δ^{13}C (‰) CH$_4$
				Aqueous concentrations			
1R-1-79	A	initial	0.0	17.0	bd	20.1	-62
1R-1-79	B	initial	0.0	17.3	bd	26.9	-64
14R-1-11	A	initial	0.1 ± 0.0	17.4	bd	27.4	-52
1R-1-79	A	1st transfer	0.7 ± 0.3	8.0	bd	1.4	-54
1R-1-79	B	1st transfer	1.6 ± 0.3	8.4	bd	2.4	-62[4]
14R-1-11	A	1st transfer	1.5	7.4	bd	2.2	-62[4]
23R-2-21	A	1st transfer	0.7 ± 0.5	7.7	bd	3.3	-65

[1] initial concentration: 15.3 mM in original enrichment medium, 1.3 mM in transfer medium.
[2] initial concentration: 2.1 mM
[3] initial concentration: ≥29.8 mM
[4] average of duplicate measurements with precision of ± 1.5‰.

Table S10. (A) Mean molar content of the potential electron donors Fe(II), S (AVS+CRS), and OC per liter of basalt. (B) Mean molar content of the potential electron acceptors Fe(III), SO_4, and IC per liter of basalt. All molar contents were calculated from mean weight percentages of Fe, S, and C fractions in host rock, and are from this study (Tables S2, S4, S13) except where indicated by footnotes. Molar contents of bulk data were converted from per gram to per liter assuming a basalt density of 2,750 g L^{-1}, which is the mean bulk density of basalt at U1301B (calculated from (9)). Molar contents of aqueous species (DOC, sulfate (aq), DIC) were calculated assuming a porosity of 5.3%, which is the mean porosity at U1301B (calculated from (9)), by multiplying mean concentrations from basement fluids sampled from boreholes or BBS by a factor of 0.053. These values are rough estimates since they assume that concentrations of basement fluids from boreholes or BBS fully reflect those within veins and basaltic pore space. CRS was assumed to be 100% pyrite (FeS_2). Abbreviations: FTT = Fischer-Tropsch-type, SR = sulfate reduction, MG = methanogenesis, AG = acetogenesis, Fe-red = Fe(III) reduction, FMT = fermentation, ND = not determined, N/A = not applicable (sample size < 3).

(A)

e^--donor	mol L^{-1} basalt		Potential energy-yielding reactions
	Mean	SD	
Fe(II)[1]	2.5E+00	2.5E-01	Indirect; biotic SR, MG, AG, Fe-red from (a) H_2 produced by serpentinization and/or (b) small organic molecules produced by FTT synthesis
Olivine[1,2]	9.1E-01	1.2E+00	
S (AVS+CRS)	3.3E-02	2.7E-02	Indirect; biotic S^0 disproportionation of S species, e.g. produced by abiotic S^{2-} oxidation with Fe(III)
AVS	7.1E-03	1.2E-02	
CRS	2.6E-02	2.3E-02	
TOC	6.2E-02	2.4E-02	Biotic SR, MG, AG; AOM, FMT
DOC[3]	6.6E-7	N/A	Biotic SR, MG, AG; AOM, FMT

(B)

e^--acceptor	mol L^{-1} basalt		Potential energy-yielding reactions
	Mean	SD	
Fe(III)[1]	1.1E+00	3.7E-01	Abiotic Fe(III) reduction by reactions with S^{2-} may restore bioavailable inorganic S species; biotic Fe-red
Sulfate (total)	9.5E-03	8.0E-03	Biotic SR, AOM
Sulfate (aq)[4]	1.0E-03	N/A	Biotic SR, AOM
IC	ND	ND	Biotic MG, AG
DIC[5]	2.0E-06	N/A	Biotic MG, AG

[1]individual values (in wt %) shown in Table S11.
[2]averaged from *9*.
[3]assumes 12.5 µM concentration, which is the average from 1026B and BBS (*6*).
[4]assumes 17.6 mM, which is value measured in U1301A borehole fluid (*11*).
[5]assumes 37.5 µM, which is the average from 1026B and BBS (*10*).

Table S11. Fe^{2+}, Fe^{2+}-olivine, Fe^{3+}, and FeTotal (FeT) content in host rock and halos (halos in parentheses) at borehole U1301B. All data from this study, except Fe^{2+}-olivine data, which was calculated from bulk olivine measurements published in reference *9*.

| Sample ID | Depth (mbsf) | weight % | | | |
		Fe^{2+}	Fe^{2+}-olivine	Fe^{3+}	FeT
1R-1-14	351.3		bd		
1R-1-79	352	4.8		3.5	8.3
1R-1-118	352.4		trace		
2R-1-4	357.1		0.7		
2R-2-98	359.6	5.4		2.3	7.7
4R-4-7	371.2	5.3		2.5	7.8
5R-1-22	377.5	5.4		1.9	7.4
6R-2-129	388.8	4.1 (5.1)		2.0 (4.5)	6.1 (9.6)
12R-1-31	429.2		5.5		
14R-1-11	434.1	5.6 (5.7)		1.7 (3.5)	7.3 (9.2)
15R-4-66	448.8		trace		
16R-1-83	454.0		2.2		
17R-1-70	462.1	4.4 (5.5)		2.2 (3.8)	6.5 (9.3)
18R-2-92	473.2		7.7		
19R-1-41	476.5	5.2 (5.1)		1.8 (3.7)	6.9 (8.9)
19R-1-132	477.4		1.7		
20R-1-57	481.2	5.0		3.7	8.7
21R-2-126	493.0		0.9		
23R-2-21	501.6	4.8 (5.9)		1.5 (1.8)	6.3 (7.8)
26R-1-41	515.9		1.1		
26R-1-76	516.3	5.8 (6.1)		1.5 (2.3)	7.3 (8.4)
35R-2-107	566.1		0.8		
36R-2-102	575.7		1.7		

Table S12. List of *dsrAB/dsrB* primers tested in study. *xdsrB* = xenologous *dsrB*, *rdsrB* = reverse *dsrB*.

Primer	Sequence (5' – 3')	Target groups	Reference
Dsr-1F	ACS CAC TGG AAG CAC G	General	*14*
Dsr-4R	GTG TAG CAG TTA CCG CA	General	*14*
Dsr 1F1	CAG GAY GAR CTK CAC CG	General	*20*
Dsr 1R1	CCC TGG GTR TGR AYR AT	General	*20*
Del1075R	GYT CVC GGT TCT TDC	δ Proteobacteria	*45*
Arch1830F	TGC TGT CNA ACA TG	*Archaeoglobales*	*45*
AG dsrF	GAG AGA GGA GCA ACR	*Archaeoglobales*	This study
AG-FC dsrR	TCG TCC CAC CAS TCC CA	*Archaeoglobales*, Firmicutes	This study
dsrB F1a	CAC ACC CAG GGC TGG	General except *xdsrB*	This study
dsrB F1b	CAT ACT CAG GGC TGG	General except *xdsrB*	This study
dsrB F1c	CAT ACC CAG GGC TGG	General except *xdsrB*	This study
dsrB F1d	CAC ACT CAA GGT TGG	General except *xdsrB*	This study
dsrB F1e	CAC ACA CAG GGA TGG	General except *xdsrB*	This study
dsrB F1f	CAC ACG CAG GGA TGG	General except *xdsrB*	This study
dsrB F1g	CAC ACG CAG GGG TGG	General except *xdsrB*	This study
dsrB F1h	CAT ACG CAA GGT TGG	General except *xdsrB*	This study
dsrB F2a	CGT CCA CAC CCA GGG	*xdsrB*	This study
dsrB F2b	TGT GCA TAC CCA GGG	*xdsrB*	This study
dsrB F2c	CAT TCA TAC CCA GGG	*xdsrB*	This study
dsrB F2d	TGT TCA CAC CCA GGG	*xdsrB*	This study
dsrB F2e	CGT GCA CAC GCA GGG	*xdsrB*	This study
dsrB F2f	CGT TCA TAC ACA GGG	*xdsrB*	This study
dsrB F2g	TGT CCA CAC TCA GGG	*xdsrB*	This study
dsrB F2h	CGT GCA TAC GCA GGG	*xdsrB*	This study
dsrB F2i	CAT CCA TAC TCA GGG	*xdsrB*	This study
dsrB 4RSI1a	CAG TTA CCG CAG TAC AT	General except *xdsrB* & *rdsrB*	This study
dsrB 4RSI1b	CAG TTA CCG CAG AAC AT	General except *rdsrB*	This study
dsrB 4RSI1c	CAG TTG CCG CAG TAC AT	General except *xdsrB* & *rdsrB*	This study
dsrB 4RSI1d	CAG TTT CCG CAG TAC AT	General except *xdsrB* & *rdsrB*	This study
dsrB 4RSI1e	CAG TTG CCG CAG AAC AT	General except *rdsrB*	This study
dsrB 4RSI1f	CAG TTT CCA CAG AAC AT	General except *xdsrB* & *rdsrB*	This study
dsrB 4RSI2a	CAG GCG CCG CAG CAG AT	*rdsrB*	This study
dsrB 4RSI2b	CAG GCG CCG CAG CAC AC	*rdsrB*	This study
dsrB 4RSI2c	CAT GCT CCG CAG CAG AT	*rdsrB*	This study
dsrB 4RSI2d	CAC GCG CCG CAA GCC AC	*rdsrB*	This study
dsrB 4RSI2e	CAT GCA CCA CAA CAA AT	*rdsrB*	This study
dsrB 4RSI2f	CAG GCA CCA CAG CAG AT	*rdsrB*	This study
dsrB 4RSI2g	CAG GCT CCG CAG CAG AT	*rdsrB*	This study
dsrB 4RSI2h	CAG GCG CCG CAG TAC AT	*rdsrB*	This study

Table S13. PCR primer combination, target group, fragment size, and DNA extracts tested. For pure cultures, 40 amplification cycles were used except where indicated. Since 4 of the original 10 sample DNA extracts from Hole U1301B had been used up for *mcrA* amplifications, only 6 DNA extracts could be checked for *dsr* presence. Due to low remaining volumes of DNA extract, we first amplified residual basalt DNA extracts with the DSR1F / 4R primer pair in a 50µL-PCR-reaction volume for 40 PCR cycles, and then used subsamples (2µL) for reamplifications in 40 cycles with the DSR1F / 4R primer pair, or nested PCR using other primer combinations. [*Dsv. = Desulfovibrio, Dsm. = Desulfotomaculum, Ag. = Archaeoglobus*.]].

Primer Combination	Target Group	Size (bp)	*Dsv. oceanii*	*Dsm.* spp. Eth2[2]	*Ag. fulgidus*	*Ag. sulfaticallidus*[3]	U1301B
Dsr-1F / Dsr-4R	General	~1,900	+	+	+	-	-
Dsr-1F1 / Dsr-1R1	General	~1,000	+	+	nd	nd	-
Dsr-1F / Del1075R	δ Proteobacteria	~940	+	nd	nd	nd	-
Arch1830F / Dsr4R	Archaeoglobales	~350	nd	nd	-	-	-
AG dsrF / Dsr4R	Archaeoglobales	~1,100	nd	nd	+	-	-
Dsr-1F / AG-FC dsrR	Archaeoglobales, *xdsrB*	~900	nd	nd	+	+	-
dsrB F1a-h / 4RSI1a-f	General except *xdsrB* & *rdsrB*	~350	-[1]	nd	+	+	+
dsrB F2a-i / 4RSI1b,e	*xdsrB*	~350	nd	+	nd	nd	-
dsrB F1a-h /4RSI2a-h	*rdsrB*	~350	nd	nd	nd	nd	-

[1] negative PCR result after 25 amplification cycles

[2] Isolate provided by Flemming Mønsted Christensen.

[3] Isolated from black rust deposit on borehole observatory at ODP Site 1026 (*46*). No published *dsrAB* sequence

References

1. W. Bach, K. J. Edwards, Iron and sulfide oxidation within the basaltic ocean crust: implications for chemolithoautotrophic microbial biomass production. *Geochim. Cosmochim. Acta* **67**, 3871 (2003). doi:10.1016/S0016-7037(03)00304-1

2. K. J. Edwards, T. M. McCollom, H. Konishi, P. R. Buseck, Seafloor bioalteration of sulfide minerals: results from in situ incubation studies. *Geochim. Cosmochim. Acta* **67**, 2843 (2003). doi:10.1016/S0016-7037(03)00089-9

3. C. M. Santelli *et al.*, Abundance and diversity of microbial life in ocean crust. *Nature* **453**, 653 (2008). doi:10.1038/nature06899 Medline

4. M. R. Fisk, S. J. Giovannoni, I. H. Thorseth, Alteration of oceanic volcanic glass: textural evidence of microbial activity. *Science* **281**, 978 (1998). doi:10.1126/science.281.5379.978 Medline

5. O. Rouxel, S. Ono, J. Alt, D. Rumble, J. Ludden, Sulfur isotope evidence for microbial sulfate reduction in altered oceanic basalts at ODP Site 801. *Earth Planet. Sci. Lett.* **268**, 110 (2008). doi:10.1016/j.epsl.2008.01.010

6. M. D. McCarthy *et al.*, Chemosynthetic origin of 14C-depleted dissolved organic matter in a ridge-flank hydrothermal system. *Nat. Geosci.* **4**, 32 (2011). doi:10.1038/ngeo1015

7. J. P. Cowen *et al.*, Fluids from aging ocean crust that support microbial life. *Science* **299**, 120 (2003). doi:10.1126/science.1075653 Medline

8. B. N. Orcutt *et al.*, Colonization of subsurface microbial observatories deployed in young ocean crust. *ISME J.* **5**, 692 (2011). doi:10.1038/ismej.2010.157 Medline

9. A. T. Fisher, T. Urabe, A. Klaus, Expedition 301 Scientists, *Proc. IODP 301* (2005).

10. B. D. Walker, M. D. McCarthy, A. T. Fisher, T. P. Guilderson, Dissolved inorganic carbon isotopic composition of low-temperature axial and ridge-flank hydrothermal fluids of the Juan de Fuca Ridge. *Mar. Chem.* **108**, 123 (2008). doi:10.1016/j.marchem.2007.11.002

11. C. G. Wheat *et al.*, Subseafloor seawater-basalt-microbe reactions: Continuous sampling of borehole fluids in a ridge flank environment. *Geochem. Geophys. Geosyst.* **11**, Q07011 (2010). doi:10.1029/2010GC003057

12. A. Schippers, B. B. Jørgensen, Biogeochemistry of pyrite and iron sulfide oxidation in marine sediments. *Geochim. Cosmochim. Acta* **66**, 85 (2002). doi:10.1016/S0016-7037(01)00745-1

13. M. W. Friedrich, Methyl-coenzyme M reductase genes: unique functional markers for methanogenic and anaerobic methane-oxidizing Archaea. *Methods Enzymol.* **397**, 428 (2005). doi:10.1016/S0076-6879(05)97026-2 Medline

14. M. Wagner, A. J. Roger, J. L. Flax, G. A. Brusseau, D. A. Stahl, *Appl. Environ. Microbiol.* **75**, 7086 (1998).

15. T. Lueders, K.-J. Chin, R. Conrad, M. Friedrich, Molecular analyses of methyl-coenzyme M reductase alpha-subunit (mcrA) genes in rice field soil and enrichment cultures reveal the methanogenic phenotype of a novel archaeal lineage. *Environ. Microbiol.* **3**, 194 (2001). doi:10.1046/j.1462-2920.2001.00179.x Medline

16. G. Zhang *et al*., Methanogen community in Zoige wetland of Tibetan plateau and phenotypic characterization of a dominant uncultured methanogen cluster ZC-I. *Environ. Microbiol.* **10**, 1850 (2008). doi:10.1111/j.1462-2920.2008.01606.x Medline

17. F. Wang *et al*., GeoChip-based analysis of metabolic diversity of microbial communities at the Juan de Fuca Ridge hydrothermal vent. *Proc. Natl. Acad. Sci. U.S.A.* **106**, 4840 (2009). doi:10.1073/pnas.0810418106 Medline

18. O. U. Mason *et al*., Prokaryotic diversity, distribution, and insights into their role in biogeochemical cycling in marine basalts. *ISME J.* **3**, 231 (2009). doi:10.1038/ismej.2008.92 Medline

19. K. Knittel, A. Boetius, Anaerobic oxidation of methane: progress with an unknown process. *Annu. Rev. Microbiol.* **63**, 311 (2009). doi:10.1146/annurev.micro.61.080706.093130 Medline

20. A. Dhillon, A. Teske, J. Dillon, D. A. Stahl, M. L. Sogin, Molecular characterization of sulfate-reducing bacteria in the Guaymas Basin. *Appl. Environ. Microbiol.* **69**, 2765 (2003). doi:10.1128/AEM.69.5.2765-2772.2003 Medline

21. G. Webster *et al*., Prokaryotic community composition and biogeochemical processes in deep subseafloor sediments from the Peru Margin. *FEMS Microbiol. Ecol.* **58**, 65 (2006). doi:10.1111/j.1574-6941.2006.00147.x Medline

22. S. Ono, N. S. Keller, O. Rouxel, J. C. Alt, Sulfur-33 constraints on the origin of secondary pyrite in altered oceanic basement. *Geochim. Cosmochim. Acta* **87**, 323 (2012). doi:10.1016/j.gca.2012.04.016

23. M. D. Rudnicki, H. Elderfield, B. Spiro, Fractionation of sulfur isotopes during bacterial sulfate reduction in deep ocean sediments at elevated temperatures. *Geochim. Cosmochim. Acta* **65**, 777 (2001). doi:10.1016/S0016-7037(00)00579-2

24. M. S. Sim, T. Bosak, S. Ono, Large sulfur isotope fractionation does not require disproportionation. *Science* **333**, 74 (2011). doi:10.1126/science.1205103 Medline

25. D. E. Canfield, B. Thamdrup, The production of 34S-depleted sulfide during bacterial disproportionation of elemental sulfur. *Science* **266**, 1973 (1994). doi:10.1126/science.11540246 Medline

26. A. L. Zerkle, C. H. House, S. L. Brantley, Biogeochemical signatures through time as inferred from whole microbial genomes. *Am. J. Sci.* **305**, 467 (2005). doi:10.2475/ajs.305.6-8.467

27. H.-T. Lin, J. P. Cowen, E. J. Olson, J. P. Amend, M. D. Lilley, Inorganic chemistry, gas compositions and dissolved organic carbon in fluids from sedimented young basaltic crust on the Juan de Fuca Ridge flanks. *Geochim. Cosmochim. Acta* **85**, 213 (2012). doi:10.1016/j.gca.2012.02.017

28. W. B. Whitman, T. L. Bowen, D. R. Boone, The Methanogenic Bacteria. *The Prokaryotes* **3**, 165 (2006). doi:10.1007/0-387-30743-5_9

29. M. A. Lever *et al*., Acetogenesis in Deep Subseafloor Sediments of The Juan de Fuca Ridge Flank: A Synthesis of Geochemical, Thermodynamic, and Gene-based Evidence. *Geomicrobiol. J.* **27**, 183 (2010). doi:10.1080/01490450903456681

30. T. M. McCollom, J. S. Seewald, Abiotic synthesis of organic compounds in deep-sea hydrothermal environments. *Chem. Rev.* **107**, 382 (2007). doi:10.1021/cr0503660 Medline

31. M. A. Lever *et al.*, Trends in Basalt and Sediment Core Contamination During IODP Expedition 301. *Geomicrobiol. J.* **23**, 517 (2006). doi:10.1080/01490450600897245

32. J. F. Biddle *et al.*, Heterotrophic Archaea dominate sedimentary subsurface ecosystems off Peru. *Proc. Natl. Acad. Sci. U.S.A.* **103**, 3846 (2006). doi:10.1073/pnas.0600035103 Medline

33. M. A. Lever, Ph. D. Dissertation, University of North Carolina at Chapel Hill, Chapel Hill, NC (2008).

34. W. Ludwig *et al.*, ARB: A software environment for sequence data. *Nucleic Acids Res.* **32**, 1363 (2004). doi:10.1093/nar/gkh293 Medline

35. E. M. Ripley *et al.*, Analytical Methods for Sulfur Determination in Glasses, Rocks, Minerals and Fluid Inclusions. *Rev. Mineral. Geochem.* **73**, 9 (2011). doi:10.2138/rmg.2011.73.2

36. P. Craddock, O. Rouxel, L. Ball, W. Bach, Sulfur isotope measurement of sulfate and sulfide by high-resolution MC-ICP-MS. *Chem. Geol.* **253**, 102 (2008). doi:10.1016/j.chemgeo.2008.04.017

37. A. Delacour, G. L. Früh-Green, S. M. Bernasconi, P. Schaeffer, D. S. Kelley, Carbon geochemistry of serpentinites in the Lost City Hydrothermal System (30°N, MAR). *Geochim. Cosmochim. Acta* **72**, 3681 (2008). doi:10.1016/j.gca.2008.04.039

38. B. N. Popp, F. J. Sansone, T. M. Rust, D. A. Merritt, Determination of Concentration and Carbon Isotopic Composition of Dissolved Methane in Sediments and Nearshore Waters. *Anal. Chem.* **67**, 405 (1995). doi:10.1021/ac00098a028

39. C. H. House, J. W. Schopf, K. O. Stetter, Carbon isotopic fractionation by Archaeans and other thermophilic prokaryotes. *Org. Geochem.* **34**, 345 (2003). doi:10.1016/S0146-6380(02)00237-1

40. S. Sakata, J. M. Hayes, M. Rohmer, A. B. Hooper, M. Seemann, Stable carbon-isotopic compositions of lipids isolated from the ammonia-oxidizing chemoautotroph Nitrosomonas europaea. *Org. Geochem.* **39**, 1725 (2008). doi:10.1016/j.orggeochem.2008.08.005

41. M. Könneke, J. S. Lipp, K.-U. Hinrichs, Carbon isotope fractionation by the marine ammonia-oxidizing archaeon Nitrosopumilus maritimus. *Org. Geochem.* **48**, 21 (2012). doi:10.1016/j.orggeochem.2012.04.007

42. K. L. Londry, D. J. Des Marais, Stable carbon isotope fractionation by sulfate-reducing bacteria. *Appl. Environ. Microbiol.* **69**, 2942 (2003). doi:10.1128/AEM.69.5.2942-2949.2003 Medline

43. K. L. Londry, L. L. Jahnke, D. J. Des Marais, Stable carbon isotope ratios of lipid biomarkers of sulfate-reducing bacteria. *Appl. Environ. Microbiol.* **70**, 745 (2004). doi:10.1128/AEM.70.2.745-751.2004 Medline

44. M. J. Alperin, T. M. Hoehler, Anaerobic methane oxidation by archaea/sulfate-reducing bacteria aggregates: 2. Isotopic constraints. *Am. J. Sci.* **309**, 958 (2009). doi:10.2475/10.2009.02

45. A. Gittel, K. B. Sørensen, T. L. Skovhus, K. Ingvorsen, A. Schramm, Prokaryotic community structure and sulfate reducer activity in water from high-temperature oil reservoirs with and without nitrate treatment. *Appl. Environ. Microbiol.* **75**, 7086 (2009). doi:10.1128/AEM.01123-09 Medline

46. B. O. Steinsbu *et al*., Archaeoglobus sulfaticallidus sp. nov., a thermophilic and facultatively lithoautotrophic sulfate-reducer isolated from black rust exposed to hot ridge flank crustal fluids. *Int. J. Syst. Evol. Microbiol.* **60**, 2745 (2010). doi:10.1099/ijs.0.016105-0 Medline